16

Basics of lead–acid battery modelling and simulation

J. Badeda [1,2,3], M. Huck [1,2], D.U. Sauer [1,2,3], J. Kabzinski [1,2], J. Wirth [1,2]

[1] RWTH Aachen University, Aachen, Germany
[2] Jülich Aachen Research Alliance, Jülich, Germany
[3] IRWTH Aachen University, Aachen, Germany

16.1 Introduction

The endeavour to model single mechanisms of the lead–acid battery as a complete system is almost as old as the electrochemical storage system itself (e.g. Peukert [1]). However, due to its nonlinearities, interdependent reactions as well as cross-relations, the mathematical description of this technique is so complex that extensive computational power is necessary to simulate the whole system in detail.

The historic development of battery models that were applied for the simulation of lead–acid battery types can be divided into three main paths; namely the one of macroscopic, mesoscopic (including macrohomogeneous) and microscopic models. Fig. 16.1 depicts the timeline of selected publications within these development paths. This overview cannot include all representative works that have been published during the last centuries but gives an idea of the most influential authors in the segment of lead–acid battery modelling.

Each of the three model categories had, and still has, its specific advantages for developers, manufacturers and researchers. Macroscopic models are mostly employed for performance relevant characterization of given systems, while mesoscopic models are more detailed on specific aspects that allow suggestions for design optimization. Microscopic models are the most detailed look at the electrochemical system and help to understand single effects in depth.

Macroscopic models are essentially a simplified description of the battery system without a detailed look into all characteristic physical specifics. The parameters are gained through measurements on the battery type treated. For online applications like battery monitoring, predefined parameter sets

Lead–Acid Batteries for Future Automobiles. http://dx.doi.org/10.1016/B978-0-444-63700-0.00016-7

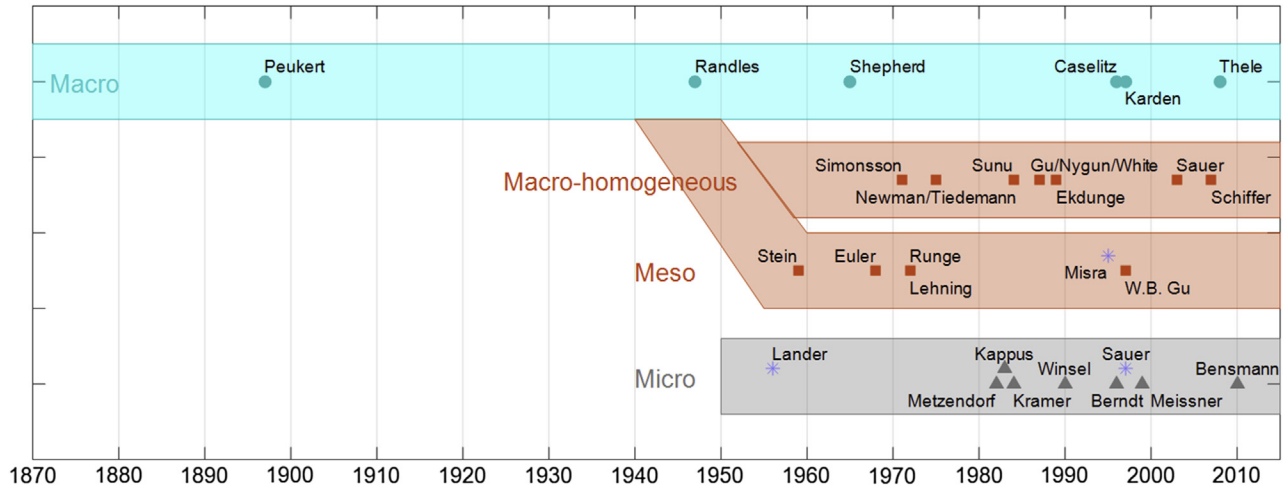

Figure 16.1
Overview of historic development of lead–acid battery modelling through selected authors. Publications marked with * cover modelling of ageing mechanisms.

may be used as initial values for model adaptation and learning. Early macroscopic models were based on empirical findings such as the influence of current rates on the available capacity described by the Peukert equation. Nowadays the description of battery performance based on Equivalent Electrical Circuits (EEC) with concentrated elements can be subcategorized in the family of macroscopic models. The work of Randles [2] can be seen as the momentum for the employment of electrical circuits in battery modelling. The parameterization of such models was first performed through measurements in the time domain and was later extended through measurements in the frequency range. In the 1960s Shepherd [3] published an equation that could be easily parameterized and extended to allow the modelling of discharge and charge behaviour [4] at constant current. In most recent works this equation was adapted mostly for charge processes.

Compared to the macroscopic models, the category of mesoscopic models goes one step deeper into the electrochemical system, which allows calculations for design optimization. Mesoscopic models assume locally homogeneous conditions and average over the exact structure (like pores). This type of model came up in the late 1950s and 1960s and was used to describe phenomena occurring on the electrode scale. Euler [5] worked on the description of porous positive lead dioxide electrodes.

During the late 1970s and the 1980s researchers such as Tiedemann, Newmann, Gu and Sunu developed macrohomogeneous models, which were used to simulate porous electrodes and full cell behaviour without the necessity to know the exact geometric details of the active-mass (AM). The current distribution and the shift of the reaction zone through a discharge or charge process was the focus of their works. Tiedemann and Newman [6] developed a one-dimensional (1D) formula to describe the change in ohmic resistance due to AM state-of-charge (SoC) and electrolyte changes. They employed this knowledge to optimize the electrode so that a maximum AM exploitation during discharge was guaranteed. Sunu [7] measured the non-uniformities of potentials under consideration of local acid densities to extend their existing model with a simulation of inhomogeneous current distribution. With this extension the influence of electrode heights and grid configurations on cranking ability was analysed. Gu, Nguyen and White [8] extended the existing models, which were mainly used for battery design optimization, to also cover the effects of rest periods, charge and cyclic processes. The description of structural changes within the electrodes was included in the work of Simonsson and Ekdunge [9], who previously also modelled the current distribution in the electrodes [10]. The most influential recent work is from W.B. Gu et al. [11]. They describe the coupled electric system with mass transport in the electrolyte. Most modern approaches are based on the work of W.B. Gu et al. Additionally, the phenomenon of acid stratification was described in more detail and with spatial resolution by Sauer [12].

Microscopic models categorize those approaches that describe processes on the microscopic ('particle') scale. This may be crystals, pores or in the extreme case molecules. Microscopic models are not used to model the battery behaviour but rather to gain information on the material behaviour for larger scale models or as submodels for batteries to calculate local parameters. The work of Lander [13] in the 1950s is a baseline for the description of corrosion processes in the lead–acid battery. The development of microscopic models took off in the 1980s and 1990s, e.g., with the description of AM utilization by Metzendorf [14] or the sulfate crystal evolution published by Kappus [15]. Furthermore, the work of Winsel [16,17] and later Meissner [18] on the aggregate-of-spheres theory can be subsumed in this category. In addition, the work of Kramer [19] on the random network model and Bernardi [20–22] on two-dimensional (2D) models and oxygen recombination has to be mentioned.

Today's level of computational power and the possibility of parallel computing allows a more detailed calculation of processes with nonlinear equations, representation of non-Faradaic currents, in all three dimensions, and higher resolution for the simulated system of a cell or complete battery. Therefore, new models evolve that allow dynamic performance characterization and design optimization as well as an in-depth understanding of inner processes in the battery [23,24]. Furthermore, the implementation of the interdependent processes within a lead–acid battery in three-dimensional (3D) models result in a deeper and more detailed understanding of the working principles behind this technology.

This chapter introduces in more detail different modelling approaches for lead–acid batteries with the focus on automotive applications. The main model types described in this chapter are quantitative models, which can be used to simulate battery behaviour for simpler problems such as calculation of a current SoC or to investigate more complex subjects such as diffusion processes. Section 16.2 offers guidance for the selection of the appropriate model level for a specific technical problem. Therefore, the different model concepts are briefly described and opportunities as well as restrictions are summarized. At the end a checklist shall help to identify the right model approach for the reader's own investigation. In Section16.3 the specific challenges for a model of lead–acid batteries are described with regard to model implementation. Especially the manifold reactions and the changing parameters with SoC and state-of-health (SoH) are discussed. The following Section 16.4 contains a description of current models used to characterize the electrical performance of lead–acid batteries. Empirical models as well as the concept of EEC and physicochemical approaches are covered. For the consideration of performance changes with reduced SoH ageing models are applied. The different concepts are described and compared in Section 16.5.

16.2 Levels of battery modelling

In general, today's models can be divided into performance characterizing so-called electrical parts and battery ageing calculating parts. For each part the level of detail defines one of three subgroups (Fig. 16.2). They consist of a mixture of the macroscopic, mesoscopic and microscopic approaches. From left to right the complexity of the model increases. The choice between model categories can be supported by the following section.

16.2.1 Defining the requirements for a battery model

There are several methods that allow a model representation of battery behaviour. To identify the right model a careful analysis of the requirements imposed by the technical problem helps to specify its necessary level of detail and accuracy. Preliminary considerations have to include the definition of the considered battery type, the operating conditions of this battery and the model boundaries. Surely, the most detailed models should be able to answer all questions. But with increasing details the number of model parameters, which need to be identified, and the computation time increase dramatically. Therefore, identifying an appropriate model is always a compromise between accuracy and implementation effort. Furthermore, the processing power available on a computer or a microcontroller has to be taken into account for the planned implementation. It makes a significant difference whether the model should run on a desktop PC, computational cluster or microcontroller as part of a battery management or battery monitoring system. The simulation environment plays a crucial role for the model implementation. This includes the possibility of the battery model being a submodule in a larger system model. For this the submodule interface has to consider necessary inputs and outputs in the overall given simulation stepsize. Next, the expected accuracy should be declared as it influences the necessary precision of modelling and parameterization procedure. Fig. 16.3

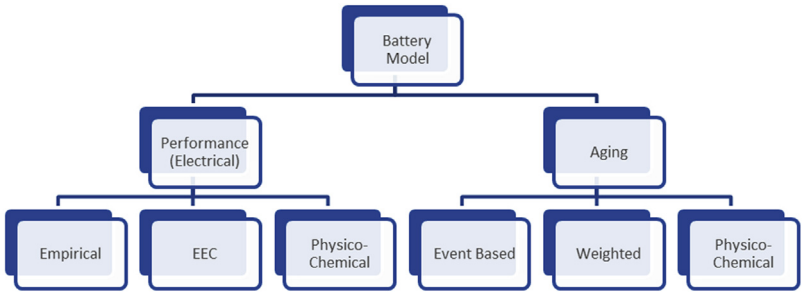

Figure 16.2
Classification of battery models into performance- and ageing-relevant approaches.

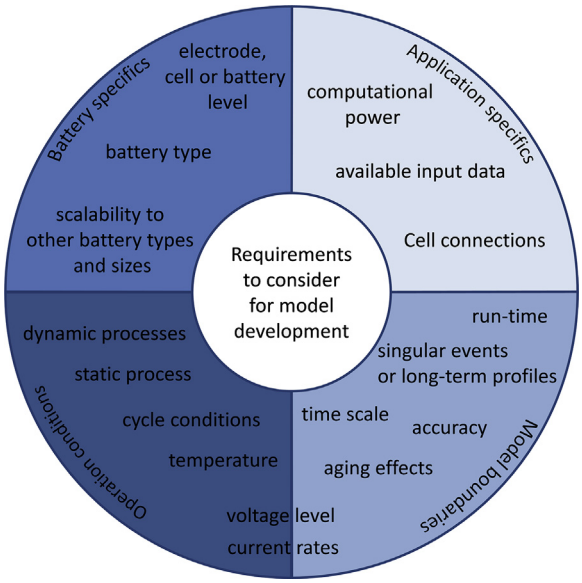

Figure 16.3
Requirements that should be considered during the development phase of a battery model.

gives an overview on the cluster of requirements, which should be considered prior to a model development.

The battery type such as flooded starting-lighting-ignition (SLI) battery, bsorptive glass-mat (AGM) SLI, UltraBattery™ or other auxiliary or traction battery has to be considered as it implies different extensions to basic model approaches. For example, if a valve-regulated lead–acid (VRLA) battery shall be analyzed, the effect of the oxygen recombination cycle on the electrode potentials cannot be neglected. And for a flooded battery a gassing and acid stratification model would be of interest, e.g., to include the influence of acid stratification. It should also be reflected whether the model shall be adaptable for a large number of different batteries or describe only one battery type as precisely as possible. This decision will subsequently determine the parameterization effort. An additional aspect that has to be taken into account is simplification of the simulation model to one cell even in cases when the considered battery storage system consists of multiple cells connected either in parallel or in series. In case of 12V SLI batteries such a simplification is broadly acceptable. However, in case of 60V UPS (uninterruptible power-supply) system with 30 cells in series and at least two strings in parallel such simplification can cause additional noticeable inaccuracies as they ignore statistical cell-to-cell variability.

The operating conditions determine another set of restrictions for the model. It should be specified if the battery behaviour shall be represented for

full cycles or if, e.g., only the discharge behaviour or even just short-term response to specific pulses shall be analyzed. SLI applications are usually characterized by shallow cycling operation around a partial state-of-charge (PSoC) that establishes during customer operation. In many laboratory or vehicle tests, SLI batteries are externally charged and slowly approach PSoC while being tested with superimposed micro-cycles. If the impact of different operating conditions should be analyzed, it is of utmost importance that the model output varies with the conditions to be analysed. If, as an example, one searches for the appropriate current rate during charging, the model must show the impact of the current rate, e.g., on the available capacity or the temperature. In case of the analysis of ageing effects, the number of implications is even higher. If cycling operation occurs and charge and discharge behaviour is investigated, it is essential to clarify how ageing behaviour shall be implemented. On the one hand, it might be of interest to simulate a long-term profile where the change in behaviour due to ageing shall be registered continuously. On the other hand, in some cases only the behaviour in a specific short-term profile (seconds or hours or even a full day) shall be compared for a new and an aged battery. Therefore, only some relevant properties which change due to ageing, e.g., the inner resistance, need to be adapted and no full ageing model has to be implemented. Besides the possible implementation of ageing mechanisms, also the relevant duration is of interest. It could be necessary to simulate milliseconds to seconds for a detailed analysis of battery performance under, e.g., cranking conditions where high current rates are applied. However, there might be analyses that cover several seconds, a day or a year. Another aspect is the given current rate (e.g., very low $<0.01\ C_{20}$ (float charging or quiescent drain), low $<0.1\ C_{20}$[1] or high $>1\ C_{20}$, very high $>10\ C_{20}$) and even more the current gradients, which determines the necessary time steps for each calculation operation. For the selection of time step size the available input data and their resolution play a role as well. Associated to this consideration is also the question of necessary computational speed in the application. For battery management systems (BMSs) or emulation of battery behaviour via hardware-in-the-loop (HiL) real-time capability is one important aspect.

Higher current rates, intensive cycling and long simulation periods require a thermal model to cover the changing thermal state of the system. It is needed to simulate the internal heat sinks and sources as well as heat exchange with the environment (radiative and convective dissipation, heat conduction via cables and contact with the floor, external heating or cooling), which have an influence on the battery performance. If durations of only milliseconds or small

[1] *In this chapter current rates are given as C-rates with the unit $A^{\circ}Ah^{-1}$. As the nameplate capacity of starter batteries is normally the 20-h discharge capacity (C_{20}), all values are referred to this capacity. The understanding is that $0.1\,C_{20}$ has the same meaning as $2\,I_{20}$.*

current rates and a controlled ambient temperature can be expected, a thermal model could be excluded. A comparison of the performance at different temperatures could also use a simplistic temperature model, in which performance influencing effects are included through adaptation factors. However, a sophisticated thermal model only makes sense if the internal states affected by the temperature, e.g., ohmic resistance of the electrolyte, diffusion processes, gassing or charge-acceptance are relevant for the simulated conditions and if they are covered by the model.

Finally, the requirements on the model output itself have to be defined. A specific question can be answered with a high accuracy by a model of reduced complexity while a broad range of problems requires a more complex model. Therefore, it should be defined at the beginning if voltage and current rates shall only be considered in specific boundaries. The complexity is also influenced by the battery cell dimensions and spatial resolution. For example, if ageing mechanisms and their interdependencies or the lead sulfate crystal distribution shall be understood in detail a physicochemical model with three dimensions would be the preferred choice. However, if only separate effects and their influence in specific directions (e.g., vertical stratification) shall be described the dimensions and subsequently simulation duration can be reduced.

In any case, the requirements and expectation regarding the results should not be higher than what the precision of the model and the model parameters can deliver.

16.2.2 Linking the requirements to the modelling approach

If the above questions are outlined in detail a decision can be made on the model approach which shall be implemented. There are three basic categories of models, namely empirical, equivalent electrical circuit (EEC) and physicochemical models [25]. The main considerations for these models are outlined in the following sections.

16.2.2.1 Empirical model

Empirical models offer simplistic solutions for quantitative comparisons between different operating conditions. Such a simple model is the Peukert equation, which is used to estimate the influence of current rates on the available capacity of a battery. For the voltage characterization typically adapted equations based on the Shepherd relation for discharge behaviour are selected. Ageing behaviour is included via a Wöhler or so-called stress and failure (S–N) curve and can be accompanied by penalties for conditions causing increased ageing or an even simpler cycle count approach is taken. Especially in long-run simulations where the ageing of a battery over several

years shall be analyzed and comparisons of different system designs or conditions are intended, such simplistic models are taken as their calculation speed is high. The parameterization effort is extremely low as most models are set up with values given by the manufacturer. Such models normally have a low accuracy and cannot be used for precise performance analysis. For new applications and battery types an adaptation is necessary. Empirical models are a good choice for a qualitative comparison of the influence of different operation conditions, e.g., on battery's ageing.

16.2.2.2 Equivalent electrical circuit

EECs with lumped elements (averaging over the spatial inhomogeneities of real porous electrodes and possibly stratified battery cells) are the most common choice for the simulation of the electrical performance of a battery. They can be extended by simplified additional models from the microscopic level to include effects such as dynamic charge-acceptance or diffusion limitations. In some cases the parameters of the electrical elements are adapted to measured values of an aged battery to mimic its behaviour. Furthermore, they built the basis for online diagnostic algorithms. Such online models contain simplified algorithms that have to be recalibrated over time based on further empirical adaptation algorithms.

The accuracy can be high if specific processes are in focus. Only with additional models high accuracy can be reached at all points of the simulation. In practice, limits for voltage accuracy are set according to the considered conditions. For a given problem, deviations of up to 400 mV per six cells may be acceptable under standard cranking conditions. The EEC allows fast simulation and thus offers the possibility to be used for online diagnostics. The parameterization effort for one battery model is classifiable in the medium range and the adaptation for new applications and battery types needs a new parameterization procedure. Nevertheless, obtained parameters should be scalable with the battery capacity if the concerned design remains unchanged. In practice, this assumption is mostly applicable for batteries produced at the same manufacturing site with AM coming from one batch.

16.2.2.3 Physicochemical model

A physicochemical model tries to include all known mechanisms through equations evolved from first principles. These include reaction kinetics of the main (storage) as well as of relevant side-reactions, electric and mass transport in porous and two-phase electrodes, and thermal effects like self-heating. Even when simplified to one spatial dimension (usually perpendicular to the geometric surface of the porous electrodes), such models are necessarily complex, usually expressed as a system of nonlinear partial differential equations and allow the analysis of the interdependencies of several effects. The programming effort and the first parameterization are labour-intensive and

time-consuming. The large number of parameters (e.g., material and structural properties as functions of SoC and temperature) require good insight and experience to sensibly choose initial parameter values and range. However, the final model is able to simulate with a high accuracy over a wide range of cell geometries and applications. The model can predict the behaviour of new battery designs and material combinations as no measurements on the specific battery should be needed for operating the model with high accuracy. As the accuracy shall be high for the analysis and the model includes nonlinear equations, which require iterative solutions, the simulation speed is typically slow. Parallelization of calculation steps can increase the speed but such models are still mostly used for offline simulations.

16.2.3 Requirements checklist for model developers

Battery models are used in diverse ways for simulations in the automotive sector. The following is a selected list of model utilizations which shall illustrate their broad variety. The applications reach from on-board battery state detection (BSD) over offline system simulation and emulation to off-board detection and highly precise models for battery design development and prescreening. All have in common a prediction of battery or single cell/electrode behaviour under defined conditions.

Online BSD are based on simplified EEC models with parameter adaptation algorithms for the detection of SoC, SoH and state-of-function (SoF).

Offline simulation can either be used to characterize the battery behaviour within a given system (here: automotive power-supply system or power-train) or as a stand-alone investigation. The offline simulation and emulation of batteries in an automotive system is often realized through software and hardware mimicking the real applications based on the theory of EEC models (emulator or HiL). System simulation outputs may be as diverse as voltage quality under various driving conditions, charge balance for component sizing, or fuel economy and emissions of micro-hybrids. For HiL or vehicle tests, a battery model can be implemented in a battery emulator as presented by Baumhöfer et al. [26]. For a more precise simulation of dynamic (0.1–100 s) behaviour of various SLI types, EEC-based models have been extended with mass transport and dynamic charge-acceptance model extensions (e.g., Ref. [27]). An example for offline simulation of battery performance at different current rates (C_{20} to cold cranking) based on general design parameters is the ISET-LAB software [28].

The following checklist in Table 16.1 is thought as a brief overview of the questions that should be asked before the development or deployment of an electrical model. They shall give a guideline on the relevant reflections and reduce the necessary effort for the developer to a minimum. The list is not at all complete and highly simplified. However, it gives an insight in necessary

Table 16.1 Checklist for model developers

Question	Physicochemical	Equivalent electrical circuit	Empirical
How accurate shall the simulation be?	Very accurate	With tolerances	Tendencies
How quick does the simulation have to be?	Slow	Medium	Fast
How elaborated can the parameterization process be?	Laboratory and test benches available	Large to medium test matrix possible	No/few tests
How flexible shall the model be regarding new battery types or applications?	High	Medium	Low
How complex can the model be for the end user?	Expert level	Advanced to expert level	Novice level
How long can the development process take?	Years	Months to years	Weeks
How precise shall operating strategies be analyzed?	Detailed	Detailed under specific conditions	Marginal
Which aspects shall be simulated? (examples)	• Detailed ageing effects • Process interdependencies • Design optimization	• Dynamic behaviour (e.g., on-board power-supply system, CCA) • Storage dimensioning	• Qualitative lifetime assessment • Floating • Storage dimensioning

considerations taken by model developers. The questions that should be asked about the ageing part of the model should be regarding the necessary accuracy (see Section 16.5).

16.3 Specific challenges for modelling lead–acid batteries

Battery modelling has evolved into a significant research field, but only a small fraction of activities in this field has recently addressed lead–acid batteries. So it is quite likely that the reader of this chapter is experienced with modelling of other electrochemical storage devices but not with technology-specific features of the lead–acid system. While these are introduced in more detail in other chapters of this book, the following section discusses them in regard to the requirements for modelling approaches.

16.3.1 Electrolyte as active-material

One striking difference between lead–acid and almost all other electrochemical storage technologies is that the electrolyte is not solely ion conducting but takes part in the main electrochemical reaction. Consequently, electrolyte properties like ion conductivity or diffusion coefficient vary as a function of SoC. Moreover, acid concentration is the dominating factor for the equilibrium cell voltage variation with SoC, while similar variations are caused by solid state effects for intercalation electrodes in lithium-ion and NiMH batteries. Due to finite conductivity of electrolyte and electrode, as well as acid concentration effects like stratification, current distribution over the plate will in reality be inhomogeneous even if all parameters are homogeneous at the start. Therefore, the naturally inhomogeneous current distribution leads to an inhomogeneous acid concentration distribution, which implies locally different equilibrium potentials. This effect is described as acid stratification, which is an acid concentration gradient along the vertical direction. It imposes a different charging and discharging behaviour in the lower and upper parts of the electrodes. The resulting terminal voltage is then a superposition of the local potentials. A simple correlation of the open-circuit voltage (OCV) with the SoC is consequently misleading (see Fig. 16.17). Additionally, the inhomogeneity in acid concentration and inhomogeneity in current distribution interact with each other. Local consumption (during discharge) or production (during charge) of sulfuric acid in the pores of both electrodes gives rise to mass transport effects. For high discharge rates the SO_4^{2-} ions are consumed faster than diffusion can deliver and the electrolyte in the pores can get depleted resulting in a reduced conductivity and an increased voltage drop. Acid stratification as such is no ageing mechanism but it changes the intensity of ageing effects. In particular, sulfation of the bottom part of the electrode is caused by local cell reactions caused by acid gradients [29] and inhomogeneous distribution of quiescent current during key-off.

In spatially discretized models, with reasonably high resolution, this different behaviour is modelled by the different local potentials (and electric parameters). Models without spatial discretization need a heuristic approximation for the cell voltage.

To simulate acid stratification one has to consider transport mechanisms such as buoyancy, diffusion as well as the electrolyte intermixing through rising gas bubbles. Buoyancy increases the stratification while gassing and diffusion counteract this tendency. It has also been shown that the size of electrolyte reservoirs above and below the electrodes have an influence on the intensity of stratification [23]. Additionally, a temperature model is helpful as all transportation mechanisms are influenced by temperature.

16.3.2 Nonlinear charge-transfer kinetics

The electrode reactions in the lead–acid system are true electrochemical conversions with significantly nonlinear Butler-Volmer kinetics, which differentiates them from intercalation electrodes and capacitive or pseudo-capacitive electrodes. As a consequence, charge transfer in lead–acid batteries cannot be modelled as a linear resistance for almost all practical applications. In case of automotive batteries, only short pulses with very high discharge rates (engine cranking or transient load peaks $>>$100 A) may allow model linearization with an error of less than 10% for the voltage drop. In addition, the Butler-Volmer characteristic is strongly asymmetric, with much stronger polarization in charge direction ($\alpha \neq 0.5$). As a result, the charge transfer does not only depend on current rate but also on the direction of current flow.

16.3.3 Charge-acceptance

Dynamic charge-acceptance in lead–acid battery is limited especially at high SoC. The absolute amount of charge-acceptance is difficult to predict and depends not only on SoC, temperature and (to a surprisingly small extent) voltage, but also on short and long-term history. For example, a freshly discharged lead–acid starter battery may easily accept, during a 10 s brake energy recuperation pulse, a charging current 10 times higher than the identical battery under otherwise identical conditions but after a couple of months normal PSoC operation in a micro-hybrid vehicle. The lack of symmetry of Butler-Volmer kinetics mentioned above cannot sufficiently explain these limitations; even a correct nonlinear Butler-Volmer model would hardly predict charging voltages around or above 14 V for an SLI battery at charging rates as high as 1 C_{20}. Most relevant, and responsible for the aforementioned effects, are non-Faradaic reaction steps, namely the dissolution of $PbSO_4$ and Pb^{2+} ion transport. Forecasting the dynamic charging currents in automotive lead–acid batteries requires sophisticated models and is a current field of research.

The small charge-acceptance ($<$1 A Ah^{-1}) means that lead–acid batteries in applications with limited charge time like photovoltaic or automotive do not typically reach the full charge condition in normal operation (some application engineers define SoC = 100% as soon as charging current falls below a threshold but this does not correspond to complete conversion of active-materials into PbO_2 and Pb). Since ageing of lead–acid batteries in PSoC differs significantly from batteries operated near full SoC, it is important that models for operation strategies design (especially charging strategies), take charge-acceptance into account.

16.3.4 Sulfation

Sulfation is a process that necessarily has to occur in a lead–acid battery because lead sulfate is the product of the discharge process at both

electrodes. However, irreversible or hard sulfation[2] describes the accumulation of lead sulfate crystals that cannot be dissolved during the application-specific operation. Dissolution of lead sulfate and diffusion of Pb^{2+} -ions in the pore electrolyte (negative electrode) or amorphous gel zones (positive electrode) precedes the Faradaic (charge transfer) reaction. In case of dissolution/transport limitation, lead ions are consumed at the same rate at which they can be replaced, and further increase of cell voltage does not accelerate charging. In addition, passive lead sulfate covers the AM and reduces the active surface at which the electrochemical reaction step can take place thus leading to a higher charge-transfer resistance. Due to its larger molar volume, it may constrict current paths in the pore electrolyte when it is accumulated preferentially near the geometric plate surface. Furthermore, the lead sulfate crystals can build a passivation layer disconnecting parts of the active-material electrically. Lead sulfate, which is bound in irreversible sulfation, cannot be accessed by the main reaction and thus corresponds to capacity loss.

Modelling the lead sulfate precipitation and dissolution is one of the most difficult tasks in the lead–acid system. To simulate the distribution of lead sulfate on a physicochemical basis, different considerations have to be taken into account. While it is possible to simulate precipitation and dissolution at great detail, these simulations take place on the scale of nano- to micrometres and thus take a long runtime for whole cells. Therefore, often mesoscopic approaches [15,20,30] are used if real application profiles need to be simulated. The approaches try to give a distribution of crystal sizes without modelling the exact position and morphology of the crystals.

Strong dependency on temperature and acid density for the dissolution process make the crystal growth sensitive on local conditions. Furthermore, the local potential influences the tendency of the redox-reaction direction. Transportation mechanisms reacting with the change in ionic concentration are essential for the simulation of crystal growth. To cover the total influence of sulfation, Ostwald ripening has to be included as it describes the crystal growth through chemical deposition, which is especially important if the influence of pause phases shall be analysed.

16.3.5 Structural change of active-mass

During discharge the active-material is transformed into lead sulfate which is an electrical insulator. While low fractions of lead sulfate alter the electric conductivity of the solid phase only slightly, reaching a critical amount means a sudden drop of several magnitudes (from $\approx 10^{4}\ S \cdot m^{-1}$ to $\approx 10^{-6}\ S \cdot m^{-1}$)

[2] *Often 'hard sulfation' is named only sulfation, but this naming lacks the distinction between the reversible and irreversible effect.*

in conductivity of the solid phase ([23], Fig. 16.4). This results in a voltage drop ('Spannungsknie'). This is more relevant for small discharge rates; for higher rates a significant voltage drop arises from electrolyte depletion.

16.3.6 Side-reactions

The lead–acid system is thermodynamically unstable. The two most relevant side-reactions for commercial batteries are corrosion of the positive current-collector and electrolysis of water. Besides, in valve-regulated lead–acid batteries (VRLA) recombination of oxygen is a relevant process influencing the potentials at both electrodes.

16.3.6.1 Anodic corrosion

In most cases, corrosion is understood as anodic corrosion of the positive grid. At the positive electrode current-collector, corrosion results in an oxidation of the lead grid into PbO_x with x taking values between 1 and 1.5[3]; this builds up a layer between the AM and the grid. This mechanism increases the inner resistance in two ways: first, through the passivating $PbO_{1–1.5}$ and $PbSO_4$ layer that has a lower conductivity than Pb or PbO_2; second, the grid dimensions decrease resulting in a reduced cross-section and subsequently a higher resistance of the grid itself. The mechanism is an irreversible ageing effect, which means that the corrosion product cannot be reversely integrated into the grid. The volume increase due to the oxidation of lead leads to an expansion of the grid in all spatial directions. The consequences are disintegration of the active-material due to mechanical stress, macroscopic deformation of the electrode (plate growth, cupping) and possibly short-circuits after separator puncture or when growing positives get in contact with the negative cast-on-straps (COS) collector.

Corrosion is influenced by the local potential at the positive grid. In the 1950s, this was shown for pure lead wires by Lander for the first time. The corrosion rate can be evaluated as the ratio of weight loss (ΔW in mg cm^{-2} h^{-1}) over a given time (Δt) (Fig. 16.5).

The corrosion rate is positively correlated with temperature. Frequently a simple Arrhenius approach is implemented in models. The corrosion rate may then be correlated to a maximum corrosion layer thickness and a corresponding increase in ohmic resistance (Ref. [4])[4].

[3] *In a final step PbO_2 is built. This stoichiometry will subsequently be available for the main reaction as active-material.*

[4] *It should be mentioned that in the field, the resistance increase is overlaid by several effects and can hardly give an accurate indication for corrosion.*

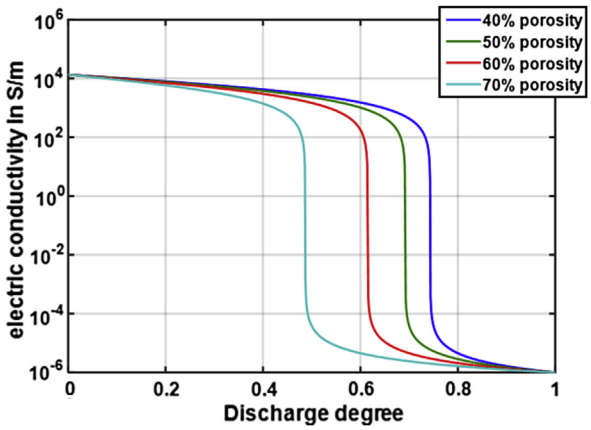

Figure 16.4
Conductivity over discharge degree in the positive electrode for different porosities.

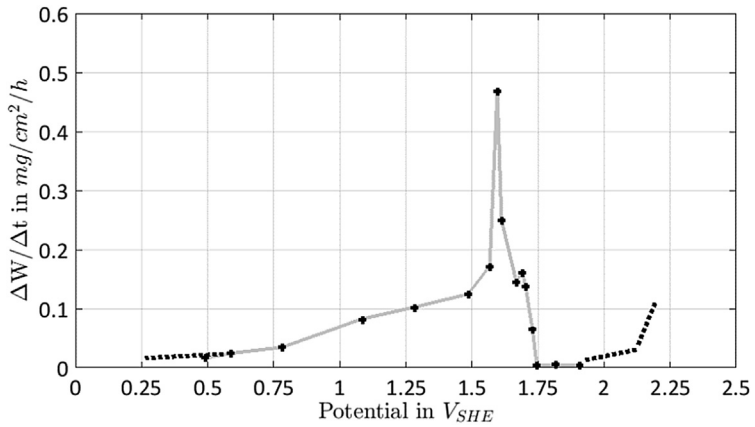

Figure 16.5
Corrosion rate depending on the potential of the positive electrode in 30% sulfuric acid based on weight loss measurements by Lander [13].

Besides its influence on the local potential (Section 16.3.1), the acid density of the electrolyte in contact with the corrosion interface changes the corrosion rate as higher availability of H_2O for the corrosion reaction will cause higher corrosion rates. This is so far neglected in the known models. In reality each grid alloy (e.g., lead–calcium) and its obtained grain structure will influence the rate of corrosion. This effect is sometimes simply included by factors adapting the corrosion rate curves based on the results of Lander.

The corrosion process, where Pb is oxidized in a reaction with H_2O, is a second source for water loss besides electrolysis. This effect should be

included in a model as a factor for acid density change. The simulation of corrosion can be neglected if only the electric behaviour is modelled and the change in the resistance is tracked with parameter adaption.

16.3.6.2 Electrolysis

The electrolysis of water occurs at both electrodes resulting in an additional charge transfer parallel to the main reaction. Only in the unique case of continuous overcharging, which automotive batteries may only experience in laboratory but never in vehicles, water electrolysis will occur in approximately stoichiometric proportions (the approximation requires corrosion to be neglected). Nevertheless, modelling as a cross-cell reaction is widely used and allows reproducing empirical charge factors (the inverse of Coulombic charging efficiency) for a given range of (micro-) cyclic applications. For detailed analysis of effects like dynamic charge-acceptance (DCA) limitation, it will be necessary to model the hydrogen and oxygen half-cell reactions. Both half-cell reactions may be described in the Tafel approximation (Eq. 16.1) because the equilibrium potentials of both main reactions draw the mixed potential into 'gas evolution' by several hundred millivolts each:

$$i_{\mathrm{gas}} = j_{0,\mathrm{gas}} A \, \mathrm{e}^{\frac{\alpha n \mathrm{F}}{RT\left(\Delta\varphi - \varphi_{0,\mathrm{gas}}\right)}} \tag{16.1}$$

Gassing is usually neglected during discharge and open-circuit condition.

With the correlation of Faraday and the amount of current flowing into the side-reaction the water loss of the battery can be calculated. In the case of stoichiometric gassing, 0.336 g H_2O are consumed per Ah of overcharge current. When electrolysis gas leaves the battery, extraction of undissociated water vapour cannot be neglected: during common overcharge conditions like 60°C, it may account for as much as a 23% increase of weight loss rates (Fig. 16.6).

Evaporation through the battery case and degassing labyrinths is usually neglected in battery simulation models.

16.3.6.3 Oxygen recombination cycle

In valve-regulated batteries the electrolyte is immobilized. Oxygen produced at the positive electrode may reach the negative electrode through gas channels in the AGM (or gel) separator and be recombined there, causing depolarization of the negative electrode and a potential shift towards the positive. Consequently the negative electrode gets undercharged and corrosion may be intensified at the positive electrode [31].

Modelling recombination consists of two steps: the transport of the educts to the electrodes and the actual reaction. For the reaction, models are given

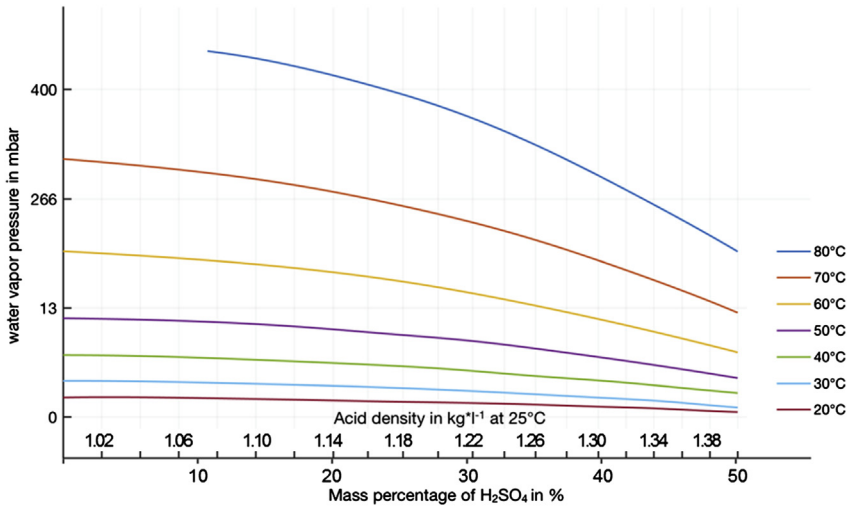

Figure 16.6
Water vapour pressure dependence on acid density at different temperatures. *Taken from D. Berndt, Bleiakkumulatoren, 11., neubearb. u. erw. Aufl., VDI-Verlag, Düsseldorf, 1986.*

by Newman [32] or Gu [33]. The transport mechanism is not fully described yet. It is assumed that some kinds of pore structures (gas channels) are built over time through which the gas diffuses to the electrodes. How these structures are evolving, particularly during micro-cycling operation, is not modelled at the moment and its understanding is topic of current research efforts.

Water loss (Section 16.3.6.2) is never completely suppressed in VRLA batteries: grid corrosion that occurs over life must be balanced by its Faradaic equivalent of hydrogen evolution, and during transient conditions hydrogen gas evolution may set in before oxygen that could be recombined reaches the negative electrode. Hydrogen recombination is usually neglected. VRLA batteries are much more sensitive to water loss than their flooded counterparts because capillary effects will draw the remaining electrolyte volume preferentially into the electrode pores, leading to dry out and eventually passivation of the upper part of the cell.

16.3.7 Implementation of side effects in battery models

Several models include one or more of the earlier-mentioned side effects. Table 16.2 gives an overview of the main influencing factors for corrosion, sulfation, water loss and acid stratification. Furthermore, an implication is given for model developers on effects that have to be considered in applications and some relevant sources for models and measurements are listed.

Table 16.2 Side-reactions and why they should be modelled with reference for model approaches

Effect	Influencing factors	Should be considered for which purpose	Sources for models
Corrosion	Temperature Acid density through influence on water proportion and local potential	Behaviour at high current pulses Capacity fade due to active-mass (AM) loss Calculation of electrode expansion for short-circuit estimation and pressure on the cell housing	[4,31,48] Measurements: [49]
Sulfation	Temperature, load profile (e.g., current rate, rest periods)	DCA, capacity loss, resistance change	[4,21]
Water loss	Temperature, load profile (e.g., full charge durations)	OCV estimation algorithms, lifetime estimation, SoC estimation, efficiency and charge factor, thermal runaway (VRLA)	[22,31,32] Measurements: [40]
Stratification	Temperature, load profile (e.g., DoD, current rate, full charges)	OCV estimation algorithms, sophisticated ageing model, detailed voltage response	[37]

DoD = depth-of-discharge = 1 − SoC.

16.3.8 Time constants

In lead–acid batteries many different effects with different time constants occur. The interaction between charge transfer and double layer capacitance of the negative electrode has a time constant in the order of milliseconds while the positive electrode has a time constant of several seconds (the exact value depends on SoC, temperature and applied load; the value for the positive electrode extends in most cases from 1 s to above 30 s). This implies that the negative electrode, which responds nearly immediately to voltage changes can be approximated with its stationary value for most profiles except those with dynamics in the millisecond scale. The time constants of the positive electrode can normally not be neglected for dynamic profiles like micro-hybrid vehicle driving cycles. There are additional effects with time constants up to several hours that are not associated with the charge transfer such as diffusion of the electrolyte between reservoir and pores, recombination cycle, hydrodynamics of gas bubbles or the transformation of intermediate amorphous structures to crystalline structures.

16.3.9 Reproducibility

It has to be mentioned that lead–acid batteries (especially flooded SLI) have much higher production tolerances than lithium-ion systems to keep the

production cost low. This means parameters like inner resistance, capacity and average acid density (and therefore the OCV) can differ noticeably for the same type of battery of the same manufacturer. Moreover, even the same battery subjected to exactly the same test profile may yield a different response the other day, as a result of some of the very slow relaxation processes described in the previous section.

When modelling lead–acid batteries this has to be kept in mind as any model can never have a better accuracy than these tolerances. Through the strong nonlinear behaviour these variances propagate into other parameters during cycling and ageing. This also means it is difficult to obtain consistent parameter sets since the batteries under test have to be treated in exactly the same way to be considered in the same state.

16.4 Models for electrical performance

16.4.1 Empirical and phenomenological models

If only the battery behaviour at the terminal under quasi stationary (constant current) conditions is of interest, simple approaches based on empirical equations as developed by Peukert [1] for capacity as a function of discharge rate or Shepherd [3] for discharge voltage curves over time may be sufficient. These calculation approaches are discussed briefly in this section. However, for most automotive simulation tasks, quasi stationary conditions do not apply.

16.4.1.1 Peukert's approach

To calculate the capacity available for discharge at different discharge current rates, simple relations based on the Peukert equation [1] can be used:

$$I^n \cdot t = I_N^n \cdot t_N \tag{16.2}$$

The Peukert Eq. (16.2) relates the discharge duration t at a certain current I with known discharge duration t_N at a known discharge current I_N (typically the nominal current) using Peukert's constant n. Peukert's constant depends on the type of lead–acid battery used (and is also influenced by the end-of-discharge voltage, especially if relatively high values are chosen). It can be determined by measurement of at least two capacities at different current rates. A typical dependency of capacities on discharge current rates is shown in Fig. 16.7 for a stationary OPzS[5] battery with 25 Ah nominal capacity at a discharge rate of 2.5 A. The resulting capacities at the given current rates are also shown in a double logarithmic plot in Fig. 16.8.

[5] *OPzS equals a flooded stationary battery with tubular plates for the positive electrode.*

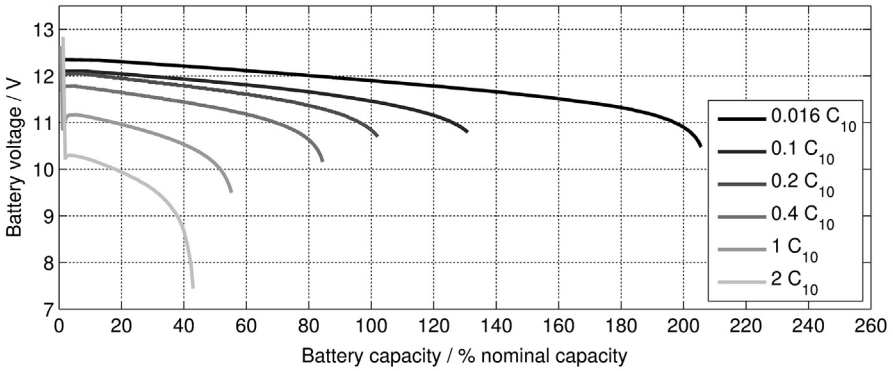

Figure 16.7
Voltage response and corresponding discharge capacities at different discharge current rates.

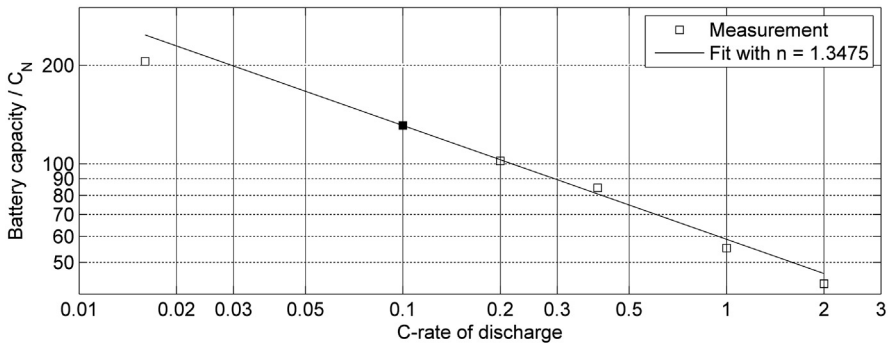

Figure 16.8
Double logarithmic representation of discharge capacities at different discharge current rates with fit using measured capacity at 0.1 C rate as fix point.

16.4.1.2 Shepherd's approach

For quasi stationary modelling of the battery voltage during discharge and charge, models based on Shepherd's equation can be used. The basis of these so-called Shepherd models is an empirical equation describing a discharge curve – voltage over SoC or time. A recent implementation of a model based on Shepherd's approach was published by Schiffer et al. [4]. The authors modified and extended the Shepherd equation resulting in Eq. (16.3) for the voltage during discharge and Eq. (16.4) for the voltage during charge:

$$U(t) = U_0 - g\,\mathrm{DoD}(t) + \rho_\mathrm{d}(t)\frac{I(t)}{C_\mathrm{N}} + \rho_\mathrm{d}(t)M_\mathrm{d}\frac{I(t)}{C_\mathrm{N}}\,\frac{\mathrm{DoD}(t)}{C_\mathrm{d} - \mathrm{DoD}(t)} \tag{16.3}$$

$$U(t) = U_0 - g\,\mathrm{DoD}(t) + \rho_\mathrm{c}(t)\frac{I(t)}{C_\mathrm{N}} + \rho_\mathrm{c}(t)M_\mathrm{c}\frac{I(t)}{C_\mathrm{N}}\,\frac{\mathrm{SoC}(t)}{C_\mathrm{c} - \mathrm{SoC}(t)} \tag{16.4}$$

In Eqs (16.3) and (16.4) $U(t)$ and $I(t)$ represent the battery voltage and current during discharge and charge. U_0 represents the OCV in fully charged state, g the slope of the open-circuit, which decreases with increasing DoD, and C_N the nominal capacity. Other parameters use different values for charging and discharging. The parameters $\rho_d(t)$ and $\rho_c(t)$ represent the battery's effective ohmic resistance for discharging and charging, respectively. These parameters are a function of time to cover battery ageing. The parameters C_d and C_c are normalized discharge and charge capacities of the battery and may also be implemented time-dependent if capacity losses because of ageing are modelled. M_d and M_c are charge-transfer overvoltage coefficients. The parameters C_d, M_d and C_c, M_c are most influential when the battery is nearly fully discharged or charged, respectively. When determining parameters, model users should keep in mind that despite its physical motivation these models are empirical and parameters determined by curve fitting can deviate from the actual values.

The simplicity of this approach does not account for the varying behaviour due to different reaction rates in discharge and charge mode. Therefore, the two equations may require an entirely different set of parameters even for the voltage U_0 and the slope g of the voltage curve [4].

16.4.2 Equivalent Electrical Circuit models

Electrical models are generally used to describe the dynamic behaviour of current and voltage at the terminals of a battery, regardless of the precise physicochemical processes within the cells. Compared with empirical approaches electrical models offer a higher accuracy with marginal parameterization effort, compared with a physicochemical model. Electrical models are based on EEC that can be represented and solved numerically in common computer modelling and simulation programmes. There are two main characteristics that are represented in a basic EEC of a lead–acid battery: the thermodynamic equilibrium voltage U_0 and the complex battery impedance. When a discharge (load) or charge current flows through the terminals, voltage drops (overvoltages) across the impedance terms are added to U_0. When the current stops flowing, the overvoltages will dissipate slowly (with some very long time constants particularly after charging, cf. Section 16.3.8). Consequently, the OCV or terminal voltage under zero external current is not generally equal to the equilibrium voltage U_0.

Both U_0 and the impedance depend on the state of the battery. In addition, the complex impedance shows strong dependencies on temperature, current rate and previous charge and discharge history. Finally, the SoH or ageing also affects both U_0 characteristics and impedance (see Section 16.5.4).

A basic element of many EECs for batteries is the so-called 'Randles equivalent circuit' [2], as depicted in Fig. 16.9. It consists of a double layer

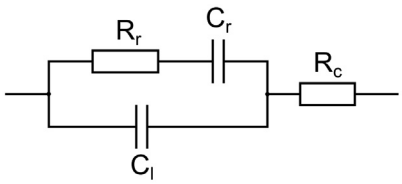

Figure 16.9
Randles equivalent electrical circuit. *Adopted from J.E.B. Randles, Discussions of the Faraday Society 1 (1947) 11.*

capacitance C_l in parallel to a series connection of a reaction resistance R_r and a reaction capacitance C_r, all in series with a series resistance R_c that represents the ohmic resistance of the electrolyte.

A common modification of Randles EEC is the usage of a constant phase element (CPE) instead of a capacitance in an RC circuit, which is then called a ZARC element and mimic the measured complex impedance more accurately (see Section 16.4.2.2).

The number of elements is chosen depending on the demand for simulation accuracy, model complexity and parameterization effort. If positive and negative electrodes are modelled separately, one RC circuit and a ZARC element can be used to represent the negative electrode and one RC circuit for the positive electrode. Such a model proposed by Thele [34] with several extensions is depicted in Fig. 16.10. Beside the main reactions, the gassing reaction is also modelled separately for both electrodes by the Tafel equation to improve accuracy for charging processes.

Depolarization due to oxygen recombination at the negative electrode is significant in VRLA batteries and is considered as well. In the following, the backgrounds of the main reaction elements are explained in more detail.

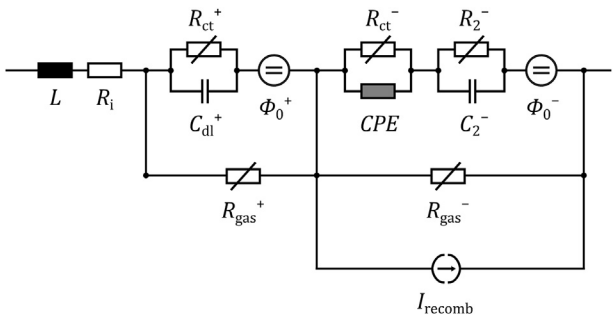

Figure 16.10
Equivalent Electrical Circuit (EEC) proposed by Thele [34] for separated representation of positive and negative electrode and gassing including recombination in VRLA batteries.

16.4.2.1 Voltage source

The equilibrium potential U_0 can be represented by a voltage source. It is highly dependent on acid concentration and therefore on SoC of the battery. For a narrow SoC range, the voltage can be linearized at a specific working point. However, if acid depletion effects have to be modelled, the nonlinear region at low concentrations cannot be neglected. If detailed information about acid density and acid amount is available, the voltage source can be modelled by the relation between the SoC-dependent acid density within the battery cell (or electrodes, if electrolyte transport effects are considered). Without detailed information, U_0 can be fitted to SoC by measurements. For this, the battery has to be discharged to different SoC and the OCV registered after a sufficiently long relaxation time. Charging the battery to a certain SoC is not recommended here because relaxation times are significantly longer. Additionally, initial capacity tests can influence the measured voltages due to postformation and acid stratification.

16.4.2.2 Constant phase element and ZARC elements

EECs designed to model behaviour of the processes taking place at electrodes make use of lumped elements of resistors, capacitors and inductors. In Nyquist plots of impedance measurements of lead–acid battery electrodes against reference electrodes (see Fig. 16.12), depressed semicircles are often observed, with a depression that can be explained by the spatial expansion of electrodes.

These depressed semicircles cannot be represented by a finite number of the lumped elements mentioned earlier. For their representation, more general definitions of complex impedances than capacitors and inductors can be applied. One example of such a more generally defined element is a CPE. For this the impedance spectrum in the complex plane still forms a line – but any angle from −90 to 90 degrees can be chosen.

The generalized RC element that is formed by a CPE and a resistor is commonly referred to as a ZARC element as its representation in the complex impedance plane is an arc. A Nyquist plot of a ZARC element is shown in Fig. 16.11 for different phase angles ξ_z of the CPE. Various phase angles ξ_z occur depending on the degree of depression of the semicircles, which is caused by the superposition of different time constants.

The complex impedance of a ZARC element is described by Eq. (16.5) [35]:

$$Z_{\mathrm{ZARC}} = \frac{R_0}{1 + R_0 A\,(j\omega)^{\xi_z}} \tag{16.5}$$

Despite their elegance in the frequency domain, ZARC elements have no closed representation in the time domain. For simulation models, their

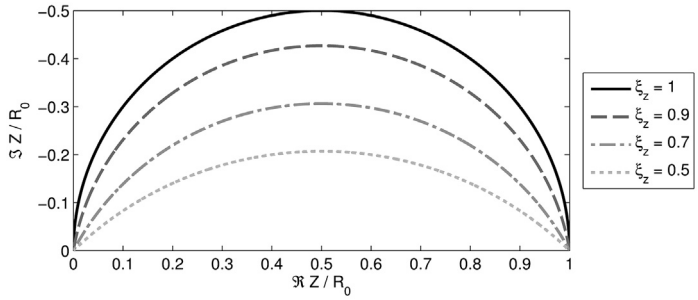

Figure 16.11
Nyquist plot of a ZARC element.

behaviour can be approximated by a series connection of (resistance (R) and a capacitance (C)) RC elements. The quality of the approximation increases with the number of RC elements.

16.4.2.3 Nonlinear Butler-Volmer resistance

The complex impedance of lead–acid batteries shows a high influence of (DC) currents on the charge-transfer resistance at all SoC and temperatures. In general, it decreases for increasing currents. This nonlinear behaviour can be described by the Butler-Volmer resistance that is given by differentiation of the Butler-Volmer Eq. (16.6):

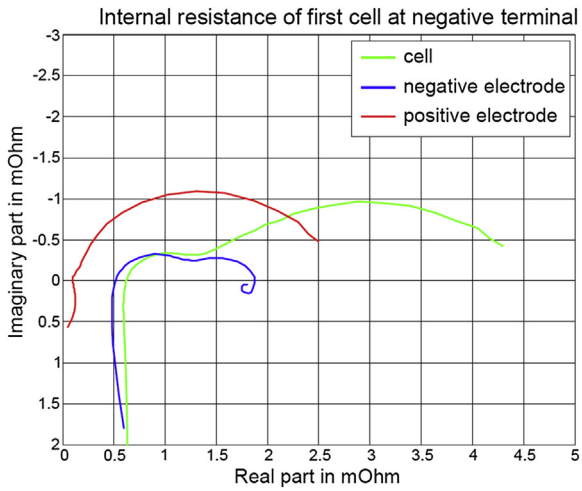

Figure 16.12
Impedance spectra for an automotive Enhanced Flooded Battery (EFB), 60 Ah, at 25°C, 70% SoC and a superimposed DC current of $-I_{20}$.

$$R_{ct}^{-1} = \frac{\mathrm{d}i}{\mathrm{d}\eta_{\mathrm{act}}}$$
$$R_{ct}^{-1} = i_0 \cdot \frac{n\mathrm{F}}{\mathrm{R}T}\left[\alpha \cdot \exp\left(\alpha \cdot \frac{n\mathrm{F}\eta_{\mathrm{act}}}{\mathrm{R}T}\right) + (1-\alpha)\cdot \exp\left(-(1-\alpha)\cdot \frac{n\mathrm{F}\eta_{\mathrm{act}}}{\mathrm{R}T}\right)\right] \quad (16.6)$$

F is the Faraday constant, R the universal gas constant, T the absolute temperature of the battery and i_0 the exchange current density at the boundary of AM and electrolyte. The first exponential term corresponds to the anodic reaction and the second exponential term to the cathodic reaction. Both reactions take place simultaneously, but at different rates, which depend on activation overpotential. The number n of electrons involved in the charge-transfer reaction is 2 for lead–acid batteries at both electrodes, and the symmetry factor α usually 0.3. This indicates that charge-transfer resistance is higher for charging than for discharging.

It has to be strongly emphasized that the nonlinearity of Butler-Volmer kinetics has a very significant effect for typical applications of automotive batteries, not only for cranking and other high-rate pulses but also for very common discharge and charge currents like 0.5 C_{20} rate. A linearization approach for 'the DC resistance', as commonly used for other battery chemistries, for lead–acid batteries will, at the very best, result in rough approximations for narrow ranges of discharge rates and durations. A more complete version of the Butler-Volmer equation is used in physicochemical approaches and does also consider the concentration dependencies (see Section 16.4.3.3).

16.4.2.4 Parameterization via Electrochemical Impedance Spectroscopy

Electrochemical Impedance Spectroscopy (EIS) is a valuable tool to characterize the complex impedance of a battery in the frequency domain. It allows deriving and parameterizing an appropriate EEC. In the galvanostatic variant, a small sinusoidal current is applied to the battery and the voltage response is registered by the measurement equipment. By varying the frequency of the sinusoidal current, the complex internal impedance of the battery can be evaluated over a wide frequency range from several kHz (above which component and circuit inductance would typically rule dynamics) down to the μHz region. It is possible to perform the measurements at different working points of the battery, mainly defined by SoC, temperature, superimposed DC current (cf. Section 16.4.2.3) and charge/discharge history.

For representative results, the battery has to be in quasi steady-state. The battery temperature has to be regulated in a water bath or climate chamber with forced air flow, and in the case of superimposed DC currents, the measurement time should be small so that the electrolyte concentration as well as the electrode condition can be assumed to be almost constant. This is

usually given by a maximum SoC change of approximately 5% during the measurement, so that the complex impedance can be evaluated in charging or discharging operation. Thus, for high superimposed DC currents the short time frame for measuring does not allow measurement of impedance spectra at very low frequencies.

Fig. 16.12 exemplarily shows impedance spectra for an automotive Enhanced Flooded Battery (EFB) cell as well as for the positive and negative electrode separately at one specific working point. Measurement of half-cell impedances requires employing a reference electrode with direct electrolyte contact in at least one cell[6]. As can be seen on the depicted Nyquist plots, the orientation of the imaginary axis is typically reversed for EIS analysis, allowing better visibility of the capacitive behaviour.

For the positive electrode, three different areas can be separated. For high frequencies, the imaginary part equals zero and the real part shows its lowest value. This point is defined by the ohmic resistances of the conductors in the battery cell, which are mainly solid lead in the grid, highly porous lead dioxide in the positive AM and the electrolyte. For higher frequencies the inductive behaviour is observed. An increasing ohmic resistance may be caused by the skin effect of the conducting parts at high frequencies. For lower frequencies, one depressed semicircle can be seen. In this frequency range, the impedance is determined by the charge-transfer processes and the double layer capacity at the interface of AM and electrolyte in the pores. Electrically, this semicircle can be represented as an RC circuit or a ZARC element if depressed. The diameter of the semicircle indicates the value of the charge-transfer resistance, whereas the double layer capacity is determined by the frequency of the RC circuit at which the absolute value of the imaginary part becomes maximal.

For the negative electrode, qualitatively similar areas can be identified, with the addition of a second semicircle. The first semicircle at high frequencies is usually depressed and can be modelled by a ZARC element. It is associated with charge-transfer kinetics. The processes governing the second semicircle, which in the cell spectrum (green curve) usually overlaps with the positive semicircle, are not yet fully understood. Fig. 16.13 illustrates the four areas in the spectrum and the mathematical as well as the EEC representation of the internal impedance for the negative electrode. The significance of EIS measurements for deriving and parameterizing becomes obvious.

To expand validity of the parameterized model to all relevant working points, EIS measurements at all relevant temperatures, SoC and current rates

[6] *The voltages are evaluated between negative battery pole and reference electrode as well as between reference electrode and a lead screw connected to the positive current-collector. The changed resistances due to this setting have to be considered.*

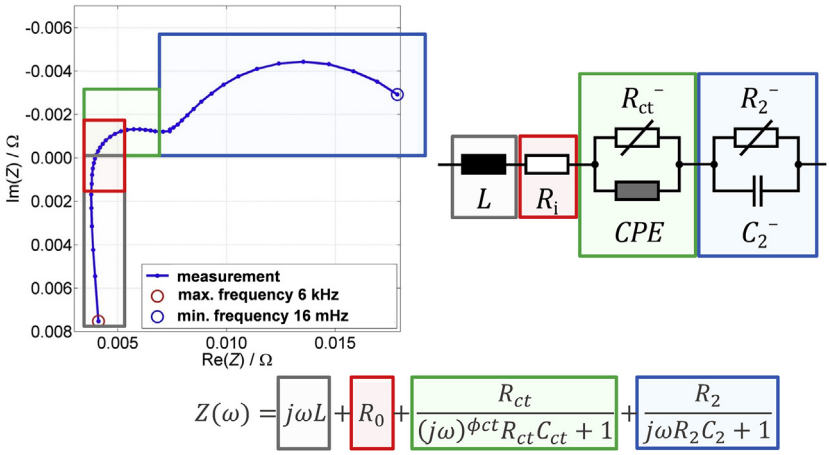

Figure 16.13
Illustration of an impedance spectrum of a negative electrode and its representation as an EEC.

have to be performed. The obtained parameters at different working points can be included as input for the model in form of regression areas.

16.4.2.5 Parameterization in time domain

The parameterization of an EEC can either be done through measurements in the frequency or in the time domain. The chosen method determines the models ability to depict large- or small-signals behaviour. If the considered time steps in the simulation are in the seconds range the EEC fitted through time-domain parameterization could be sufficient. However, the complexity of nonlinearity of the resistances in the EEC is often not covered. Time-domain parameterization plays furthermore a crucial role for BMS adaptation algorithms, which have to be adapted based on simplistic measurements in the automobile.

For currently available models also a mixture of frequency and time-domain fitting is chosen. After a first parameterization of the EEC through EIS additional parameters can be drawn from measurements in the time domain to include long-term processes more accurately. For this, the battery under test is excited through charge or discharge current pulses and its voltage responses are measured. For slow processes, which cannot be measured through EIS because the measurements would take too long and violate the requirement for a steady state, time-domain parameterization might be the only feasible way. As an example, time-domain parameterization was used by Thele [34] to determine parameters of an electrolyte transport model as an addition to an EEC model.

16.4.2.6 Simplifications for online simulation models

Due to fewer processing resources in online battery models, e.g., in automobiles, simplifications of the general EEC have to be made. These have to be carefully chosen as described in Section 16.2.2.

The main purpose of online battery models in automotive applications is to aid electrical energy management by continuously updating battery state information. This is in particular the prediction of dynamic response for certain predefined load cases (SoF) or detection of battery degradation (SoH) from electrical performance characteristics. As an example, a model could be used to predict the voltage dip during engine restart for stop–start operation and, depending on voltage quality thresholds, call an automatic restart early or inhibit engine shutdown temporarily.

As the time horizon of the prediction differs significantly for different use cases, RC and ZARC elements, as well as their nonlinearities, may be simplified for the respective load cases. Conversely, all online models can be continuously updated with measured battery current, voltage and temperature information to compensate for the lack of complex non-linear prediction capability. For example, for the stop–start SoF in engine off mode it may be found sufficient to extrapolate voltage under presently measured vehicle load for an anticipated remaining stop duration of several seconds. After which the voltage drop during typically 0.5 s cranking at very high discharge rates has to be predicted through an ohmic resistance. In offline models this resistance would be implemented as a non-linear series resistance including Butler-Volmer behaviour, while the today's online implementation uses simplifications to simulated the resulting effects.

Functional separation between battery monitoring and vehicle-side electric energy management, data interfaces like SoF and SoH, and appropriate online parameter adaptation algorithms are discussed in Section 14.3 of Chapter 14.

16.4.2.7 Limits and extensions

EECs are not fully sufficient to represent battery behaviour in certain cases. This is especially true on longer time scales if periods considered are many times larger than the time constants of the EEC. This limitation is inherent to EEC models as very low frequencies cannot be measured during EIS under quasi steady-state conditions.

To overcome these limitations, the validity range of the electrical model can be extended by addition of physicochemical submodels for certain processes. An electrolyte transport model may be realized to model deviant electrolyte densities in negative and positive electrodes and separator to cover charge depletion effects, which occur at high current discharge rates. As many of these processes, such as electrolyte transport, can be described

by simple differential equations they also could be implemented in the form of equivalent electric circuits. Thele [34] introduced an electrolyte transport model by means of voltage sources that represent the concentration of overvoltages at each electrode. The improved model accuracy in comparison to an impedance-only model is shown in Fig. 16.14. Additional physicochemical extensions have been developed to cover the influence of short-term charge and discharge history on dynamic charge-acceptance.

16.4.3 Physicochemical models

EEC based models are good at predicting the load responses under unchanged battery conditions compared with the parameterization setup. But effects which alternate the load response (like stratification, hard sulfation, etc.) have to be covered by additional parameter sets or heuristics. Physicochemical models are used when effects on different temporal and spatial scales influence the performance of the battery since these effects can be modelled together with the electric behaviour. This model type includes macrohomogeneous as well as microscopic approaches. Due to the separation of different effects and the simulation of physical variables they are suited to investigate which process do limit the battery performance.

16.4.3.1 Dimensionality

The investigation possible with a specific model is dependent on the chosen dimensions. Today's models can cover all three spatial dimensions. However, the calculation speed is highly correlated with the resolution or the intended accuracy.

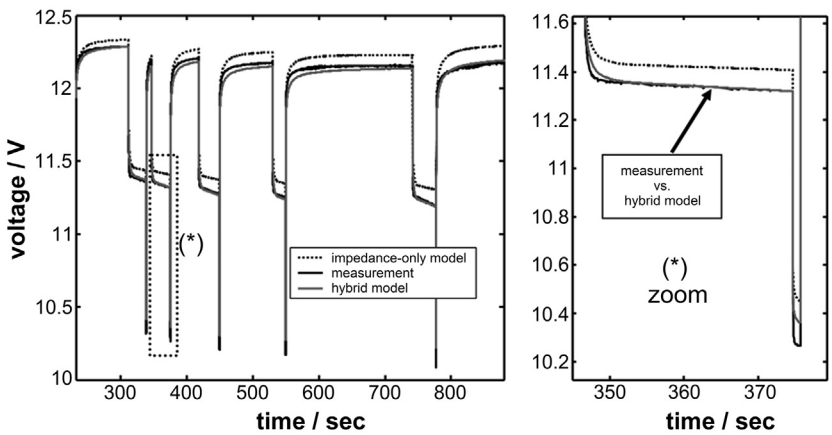

Figure 16.14
Comparison of measurement and simulation results of a hybrid model containing a transport model and an impedance-only model [37]. *From M. Thele, S. Buller, D.U. Sauer, R.W. de Doncker, E. Karden, J. Power Sources 144 (2005) 461–466.*

Most interactions take place perpendicular to the geometric electrode surfaces, which is the primary direction of current flow. This would be the natural orientation for the *x* axis in a spatially 1D model. 1D models are used to estimate the electrode/cell/battery potential. They assume that local conditions in the cell can be represented by an average, which is not applicable for tall cells and cells with high acid stratification. The grid-plate structure, with the bulk of the active-material located in grid meshes rather than on planar foils, might be approximated by a certain extension of current paths versus the geometric electrode dimensions. As a second dimension the vertical direction *z* is usually taken into account, e.g., if the variances in cell's height shall be investigated. It allows to model acid stratification, the effects of electrolyte reservoirs above and below the electrodes and the inhomogeneous AM utilization for batteries with current-collectors of both polarities solely contacted at one position of the grid (mostly at the top). The third dimension is usually taken into account for design questions as with the third dimensions the different distribution over the length of the electrodes and thus local ageing conditions are accounted for [30]. It does not alter the voltage behaviour drastically but is important for the ageing behaviour and failure mechanisms. It is also possible to consider only the two dimensions parallel to the electrode surface; this is done to design grids and electrodes, focusing on the resistive behaviour.

16.4.3.2 Implementation concepts: equivalent electrical circuit or partial differential equations?

There are two often used implementations to calculate the spatial current (or potential) distribution in the battery: EEC or partial differential equations (PDE). Both implementations can be used for one, two or three spatial dimensions, the difference lies then in the discretization method and the effects which can be described (Sections 16.2 and 16.3). The implementation as an EEC or a PDE is mostly up to personal preferences (electrical engineers usually prefer the EEC approach). The PDE approach is more flexible in the discretization and is easier to apply if the grid structure should be simulated as well. The EEC approach is based on Kirchhoff's laws. In principle both laws can be used but depending on the law used the implementation differs.

To solve the electric system, different network analysis methods can be applied. The node-voltage method aims to solve Kirchhoff's current law, which states that the currents flowing into or out of a node have to sum to zero. For this the nodal voltages are determined. With this approach the number of equations, which have to be solved, equals the number of nodes minus one.

The mesh-current method aims to solve Kirchhoff's voltage law, which states that voltages in a closed mesh need to sum to zero. For this the currents in the branches are determined. With this approach the number of equations

needed equals the number of meshes. The mesh-current method needs fewer equations and therefore can be solved in lower computational runtime.

The mesh-current method has a limitation in a three dimensional geometry. It is not possible to define closed meshes over nodes that are positioned on the corners of a dice and are connected by the edges in a linear independent way. In such cases the node-voltage method has to be used.

In both cases the electric behaviour is represented by the following elements:

- linear resistances (for the current flow in the solid matrix and the electrolyte),
- voltage or current sources (to represent the terminal load and the electrochemical potential),
- capacities (to represent the double layer) and
- nonlinear resistances (to represent the charge transfer) which are given by the Butler-Volmer equation.

An example for an equivalent electrical circuit used in a 3D model is depicted in Fig. 16.15. The resistances in one path represent the grid of each electrode, the AM, electrolyte, the charge-transfer resistance of the main reaction as well as the side-reactions such as corrosion of the positive electrode and gassing.

The PDE approach uses the charge conservation as basic equation:

$$\operatorname{div} j = 0 \tag{16.7}$$

$$j = -\sigma \nabla \varphi \tag{16.8}$$

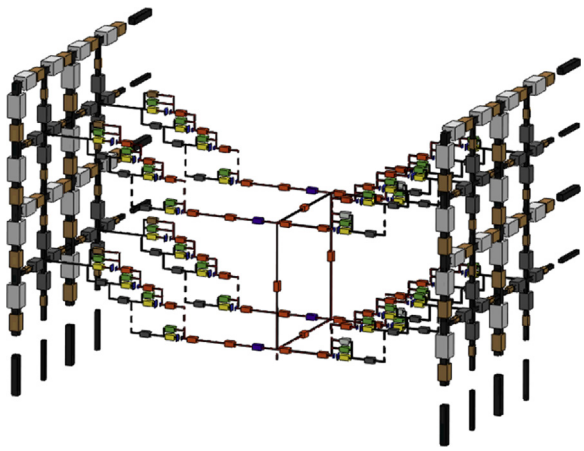

Figure 16.15
Equivalent electrical circuit three-dimensional model – resistances: grey – grid; red – electrolyte; black – active-mass; yellow – charge transfer; green – side-reaction; brown – corrosion.

In the electrolyte an additional driving force for current flow are concentration gradients.

To solve the resulting equations the boundary conditions have to be chosen appropriately:

- Neumann boundary conditions for the potential at the terminal if a current load is applied;
- Dirichlet boundary conditions at the terminal if a voltage load is applied.

The transfer between solid phase and the electrolyte is given by the Butler-Volmer equation (see Sections 16.4.2 and 16.4.3.3). This leads to the following equations in the solid and liquid phase:

$$\text{solid phase}: \nabla(\sigma_{\text{solid}}\nabla\varphi) = i(\varphi) \tag{16.9}$$

$$\text{liquid phase}: \nabla\left(\sigma_{\text{liquid}}\nabla\varphi\right) + \nabla(\sigma_{\text{D}}\nabla \ln c) = -i(\varphi) \tag{16.10}$$

where $i(\varphi)$ is the Butler-Volmer current, which is only not zero at the interface. A detailed discussion of the PDE approach is given in [11].

The conservation approach and the node-voltage method lead to the same equations for simple geometries. This is natural since Kirchhoff's current law is derived from charge conservation.

In both approaches the double layer capacity is usually neglected to increase computational performance. This means the voltage response of the electrode is immediate which is only a useful approximation for time steps $>>$10 s. The double layer capacity may be implemented in both approaches on the cost of longer runtimes.

16.4.3.3 Butler-Volmer equation

In most models an incomplete Butler-Volmer Eq. (16.11) is used:

$$i(\eta) = j_0 \mathrm{f}(\mathrm{SoC})\left(\exp\left(\frac{\alpha n \mathrm{F}}{\mathrm{R}T}\eta\right) - \exp\left(-\frac{(1-\alpha)n\mathrm{F}}{\mathrm{R}T}\eta\right)\right) \tag{16.11}$$

The factor f(SoC) is often determined empirically and often associated with concentration or active surface. The dependency on the SoC is often not physically motivated (e.g., shrinking active surface during charging). The necessity of this factor arises because the concentration dependencies are neglected. A more complete Eq. (16.12) is:

$$i(\eta) = j_0\left(\frac{c_{\mathrm{Pb}^{2+}}}{c_{\mathrm{Pb}^{2+},0}}\exp\left(\frac{\alpha n \mathrm{F}}{\mathrm{R}T}\eta\right) - \frac{c_{\mathrm{H_2SO_4}}}{c_{\mathrm{H_2SO_4},0}}\exp\left(-\frac{(1-\alpha)n\mathrm{F}}{\mathrm{R}T}\eta\right)\right) \tag{16.12}$$

This takes the local concentrations of the educts into account (the solid phases do not appear since the activity of solid matter is unity by definition).

The dependency on the Pb^{2+} concentration results in the desired charging behaviour if the Pb^{2+} concentration is modelled correctly.

16.4.3.4 Transport equations for mass and heat processes

Transport effects of mass or heat are based on the convection–diffusion equation:

$$\frac{\partial \phi}{\partial t} = \nabla A \nabla \phi - \nabla \vec{v} \phi + S \tag{16.13}$$

The diffusivity coefficient (A) in the electrolyte is a function of concentration and temperature.

Heat and mass transport have very different source terms. The source term for the mass transport is mostly given by the main reaction (a smaller contribution is given by the water production/consumption of the main and side-reaction and the volume change in the pores).

$$Pb^{2+} + SO_4^{2-} \rightleftharpoons PbSO_4 \tag{16.14}$$

This can be modelled as part of the main reaction; in this case the source term S is proportional to the main reaction current i_{MR}:

$$S = -\frac{i_{\mathrm{MR}}}{2\mathrm{F}V\varepsilon} \tag{16.15}$$

Alternatively, this can be modelled by a lead sulfate model, and then the source term depends on the nucleation and growth rate of the lead sulfate crystals. As crystal models are complex and tend to show numeric instabilities because the acid concentration influences the crystal growth rate, it is more advisable to model the acid concentration source term as current dependent to avoid oscillations.

The heat source term has many components; the most important source is the Joule heat of the ohmic resistances. The reversible heat of the main reaction is often small compared with the Joule heat and is therefore often neglected. The other important heat source (or often sink) is the exchange with the environment. This term is composed of a radiation term that follows the Stefan–Boltzmann law and the convectional heat exchange with the surrounding medium (air in most applications). For the heat exchange the heat transport in the surrounding medium has to be known (e.g., by computational fluid dynamics (CFD) simulations) or has to be approximated.

The velocity term $\nabla \vec{v} \phi$ in Eq. (16.13) is difficult to obtain. The main driving force is the buoyancy of the electrolyte. To gain the resulting velocity field the Navier-Stokes equations would have to be solved, for which the Boussinesq approximation with Darcy flow in the pores can be used [11]. Since

the velocities are small the creeping flow approximation is a further simplification [36].

An additional driving force is raising gas bubbles from the electrolysis reaction. This effect cannot be neglected if acid stratification is of importance for the application. The rising bubbles mix the electrolyte and reduce acid stratification. At the moment there is no first principle description of the bubbles and their behaviour in the electrolyte or on the active electrode surface. An empirical formula is given by Kowal et al. [37].

16.4.3.5 Transport in pores

The electrodes are porous structures that alter the diffusion and current flow behaviour, compared with free electrolyte or a massive solid phase. For numeric simulations the exact pore structure is usually averaged out by transforming the diffusion coefficient and ionic conductivity of the electrolyte into effective quantities as functions of the porosity ε and tortuosity τ:

$$D_{\text{eff}} = f(\varepsilon, \tau) D_{\text{free}} \tag{16.16}$$

$$\sigma_{\text{eff}} = f(\varepsilon, \tau) \sigma_{\text{free}} \tag{16.17}$$

The transformation functions can be determined by microscopic simulations. One simple approach is to take the reduced pore diameter into account which hinders the transport processes:

$$f(\varepsilon, \tau) = \varepsilon^{\tau} \tag{16.18}$$

For high current rates the present concentration inside the pores is more relevant, since it may significantly differ from the bulk electrolyte. This results in increased ion resistance, which is the cause for the lower available capacity for high-rate discharges. There are different approaches to handle the pore structure. If the values inside the pores are required as output values, then more sophisticated models that represent the geometrical structure have to be employed.

16.4.3.6 Active-mass utilization

The electric conductivity of the electrode material is more complex than the electric conductivity of the electrolyte since not only the porosity is important but also the amount of lead sulfate, which is an insulator, in the mass. Metzendorf [14] has formulated an approach for the lead–acid battery based on the effective medium theory, which takes into account the actual porosity and utilization of the AM.

$$\sigma_{\text{eff}} = \frac{1}{k-2}\left(Q + \sqrt{Q^2 + 2(k-2)\sigma_1\sigma_2}\right) \tag{16.19}$$

$$
\begin{aligned}
Q &= \left(\frac{k}{2}x_1 - 1\right)\sigma_1 + \left(\frac{k}{2}x_2 - 1\right)\sigma_2 \\
x_1 &= \frac{1 - r}{1 + C \cdot r} \\
x_2 &= \frac{\frac{M_2}{M_1} \cdot r}{1 + C \cdot r} \\
C &= \frac{M_2 - M_1}{M_1} \\
k &= 2\frac{(1 - \varepsilon)}{d_C}
\end{aligned}
\tag{16.20}
$$

In the formulas r denotes the (physical) discharge degree or utilization of the AM, σ_i, M_i denote the electric conductivity and the mole volume of the phase i (1 for the conducting and 2 for the insulating phase), ε denotes the porosity and d_C denotes critical mass densities, which are 0.154, 0.1 for the positive and negative electrode, respectively.

This kind of model allows predicting the incomplete utilization of the AM during discharge with small to moderate currents.

16.4.3.7 Limitations

A physical approach has many merits but also some crucial drawbacks. Only known effects can be modelled, therefore knowledge of all relevant effects is required with an accurate mathematical representation. If no physical motivated equation for a missing (and relevant) effect is available, it may be approximated by an empirical equation or a physical equation has to be developed. This has to be balanced with the performance requirements of the simulation software. Including more effects does increase the accuracy and validity range of the model but decreases the runtime performance. This trade-off has also to be considered with regard to the resolution of the discretization scheme; a high resolution (in time and/or space) increases the accuracy but decreases the runtime performance.

On the other side, the model has to be linked to reality. All models need parameters that are often low-level material parameter in the case of physical models (like diffusion coefficients, conductivity or surface tension). These parameters are often not easily accessible and need laboratories with special equipment. This is also true for verification purposes, where also the model output on local scale for, e.g., electric potential, electrolyte concentration or morphology distribution of the lead sulfate has to be investigated. There are often no or only expensive methods to gather this information. Therefore, the models can only be validated by the external (voltage–current) responses, which are super positioned from many effects.

16.5 Models for battery ageing

16.5.1 Motivation for ageing models

Electrochemical systems such as batteries age over their lifetime. The ageing mechanisms can be divided into those occurring over time under open-circuit or float conditions and those influenced by cycling operation. These two categories are called calendrical and cyclic ageing. The first are mainly influenced by temperature and voltage level, at which the battery is stored. The latter comprises the influences on the parameters of the battery caused by operation specifics such as current rate and depth-of-discharge.

The necessity for ageing models awakes out of two concepts. First, the ageing occurring due to specific operating conditions shall be understood in depth. Therefore, ageing models are mostly applied in simulations with timelines of several years. Most of the time, short dynamic pulses in the millisecond range are ignored for the calculation of ageing. Second, the electrical performance of a battery at different stages of ageing shall be simulated so that constraints and limitations can be determined before application. The parameters changed through battery ageing alter the characteristic electrical behaviour of the electrochemical system under a given load profile.

Applying ageing models helps to plan the operating strategy and the overall system design, e.g., the sizing of the battery and its components as well as the topology of the battery system.

16.5.2 Ageing mechanisms

Several ageing mechanisms occur during the lifetime of a lead–acid battery. They can be classified as reversible and irreversible. The latter include also the portion of sulfate that cannot be reversed through the standard charging in operation. All aspects of complexity to model these mechanisms are described in Section 16.3. The most important effects in modern automotive application are [38,39]:

- Cyclic wear of the positive AM;
- Anodic corrosion of the positive grid and occasionally oxidation of the negative cast-on straps (especially in VRLA) and lugs, which may eventually lead to cell shorts caused by grid growth;
- Sulfation, predominantly of the negative electrode;
- Water loss due to electrolysis, which may terminate the life of flooded batteries only in extreme cases, but significantly reduces conductivity and mass utilization after dry out in VRLA-type batteries.

In addition, short-circuits through dendrites can be detected in tear-down analysis [40] but this effect is normally neglected in ageing models. This is

due to the random occurrence of the dendritic structures and the unpredictable size of the dendritic formation. Models normally cover constantly evolving mechanisms and neglect random failure modes. Generally, the considered ageing mechanisms all result in a change of the electric characteristics of the system.

An additional process is the emergence of a vertical gradient in acid density, well-known as acid stratification [41]. This effect is not defined as an ageing mechanism in itself but it does influence the intensity of the other mechanisms.

A more detailed description of the ageing mechanisms can be found in [42–44]. Here, a simplified overview is given on the general correlation between operation parameters and the considered ageing mechanisms (Table 16.3).

16.5.3 Categories of ageing models

Battery ageing models can be classified into three major categories [25]:

1. event-oriented model
2. weighted capacity-throughput model
3. physicochemical model

In the event-oriented approach, events are classified according to their cycle depth and their individual influence on capacity loss. The sum of the single events equals the total capacity reduction. Calendrical ageing can overlay this process. The simulation is usually performed until a defined end-of-life criterion (e.g., 80% reserve capacity) is reached. As a result the electrical behaviour will be changed due to the reduced capacity of the battery. The influence of the cycle depth on the ageing behaviour can be parameterized based on cycle-life test data published by the manufacturer in the data sheet. The also given calendrical lifetime predictions (e.g., 10 years at float voltage) can be overlaid (Fig. 16.16).

If the battery behaviour is simulated, the micro- and macrocycles will be counted and rated by the possible cycle number at the given DoD. One mathematical approach for this cycle counting is the so-called rainflow algorithm [45]. This approach is based on the assumptions of a Wöhler curve (or S–N curve) like behaviour of battery ageing. The concept is adopted from the mechanical engineering sector where the failure of a machinery part can be calculated over its lifetime by summing the incremental stress of individual events. For a battery this means summing up micro- and macrocycles based on the parameterized function until the total amount of possible cycles is reached. This approach is very simplistic and neglects among others the fact that the battery history plays a role in the severity of an event.

Table 16.3 Overview of the stress factors resulting from operation strategy and load requirements and their resulting influence on the relevant ageing mechanisms

Ageing effect parameter	Wear out	Corrosion	Gassing/Dry out	Sulfation
High current density	Inhomogeneous horizontal current distribution induces mechanical stress	Impact on → *voltage* level (voltage higher or lower than float voltage accelerate corrosion) and → *temperature* Increased electric field across the corrosion layer accelerates ion diffusion and therefore corrosion	Impact indirect due to increased → *voltage* level (during charging) and → *temperature*	Increases number of small crystals during discharging; without acid stratification vertical and horizontal inhomogeneity in current distribution is increased
Low current density	Very inhomogeneous current distribution in vertical electrode direction	Low discharge current shifts → *voltage* in a zone of accelerated corrosion	No impact known	Increases growth of large crystals at the expense of small crystals; creates only few new crystals during discharging
Voltage	High voltage increases gassing and therefore mechanical stress by gas bubbles on loosened material	Lowest under float condition, increased for charge and discharge	Exponential increase in gassing rate with increasing voltage	High charging voltage helps to dissolve large sulfate crystals
Acid stratification[a]	Inhomogeneous SoC through change in current distribution	Impact on local → *voltage* and → *current* density	Impact on→ *voltage* level	Intensifies charging in top part and discharge in lower part of the electrodes, local elements lead to redistribution of current with further discharge of lower part
Temperature	Higher temperature increases gassing and therefore mechanical stress by gas bubbles on loosened material	Increased reaction rate with increased temperature	Exponential increase in gassing rate with increased temperature	Faster recrystallization resulting in larger crystals (during discharging and rest periods); increased dissolution rate of sulfate crystals with increasing temperature during charging

(Continued)

Table 16.3 Overview of the stress factors resulting from operation strategy and load requirements and their resulting influence on the relevant ageing mechanisms—cont'd

Ageing effect parameter	Wear out	Corrosion	Gassing/Dry out	Sulfation
Average state-of-charge (SoC)	The lower the SoC, the more severe is the active-mass expansion resulting in increased mechanical stress	Lower SoC results in higher solubility of Pb^{2+} ions and therefore the protecting corrosion layer dissolves faster Lower SoC equals lower → *voltage*	Lower SoC results in lower OCV and therefore reduced gassing	Lower SoC results in lower acid concentration and therefore in higher solubility of Pb^{2+} ions which speeds up recrystallization towards larger crystals
Depth-of-discharge (DoD) cycles	Higher with larger DoD due to expansion and shrinkage of active-materials	Increases corrosion because of increased change in local potential which results in change of the structure of the corrosion layer	No major direct impact	Increases growth of large sulfate crystals with low solubility
Time between complete full charging	Increased gassing (→ *voltage*) during full charge; bubbles carry out active-material and additives	Frequent full charging results in increased periods at high → *voltage* levels	Frequent full charging increases gassing and water loss	Long durations between full charging results in larger sulfate crystals with low solubility

[a]*Different acid densities with lower density in the upper part of the cell.*

The second model concept includes more testing and battery expert knowledge. In a more elaborated process, the cells are cycled at different DoD, mean SoC and temperatures and also stored at specific SoC and temperatures to analyse the cyclic and calendric ageing. In some cases also the influence of high and low current rates is investigated. Afterwards the numbers of possible cycles at the measured points of operation are base points for a regression function. As the continuous cycling tests cannot cover all aspects of ageing under real operating conditions weighting factors can be included to further take into account the following aspects:

- influence of charge/discharge history
- rest phases at PSoC
- acid stratification
- current rates at the beginning of a discharge
- duration between full charges
- deep discharges
- influence of charging strategies

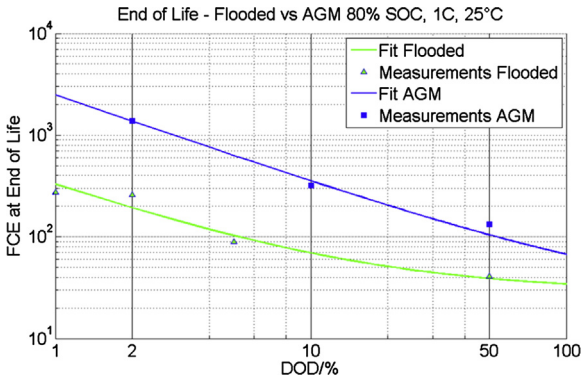

Figure 16.16
Dependency of cycle-life on depth-of-discharge. Result of a cycle tests with Flooded and AGM starter batteries. Starting SoC is always 80% of the nominal capacity, current rate is 1°C and temperature 25°C. The tests represent one single battery each. End-of-life defined as 50% remaining capacity. *Taken from J. Badeda, J. Kabzinski, D. Schulte, H. Budde-Meiwes, J. Kowal, D.U. Sauer, in: Advanced Battery Power – Kraftwerk Batterie, Aachen, Germany, February 2013.*

The test conditions have to be selected very carefully to exclude effects that shall later be included through weighting factors.

Physicochemical models are based on first principles to describe ageing processes. For example, the rate of anodic grid corrosion is influenced by the temperature, the acid density as well as the local potential in the positive electrode. The phenomenological approach tries to model each ageing mechanism separately. The basic assumptions are described in the previous Section 16.4.3. These models become very complex if they try to cover all mechanisms and aim for a high resolution. Furthermore, the parameterization process is highly sophisticated.

Both weighted throughput and physicochemical models cover a change in parameters of the electrical model such as the inner resistance or the capacity and thus consider a change in the performance of the battery over its lifetime. Table 16.4 gives an overview on the three different approaches according to their implications for the parameterization process, the speed of calculation as well as the accuracy of the results and its flexibility for a transfer on other applications or battery types.

16.5.4 Change of parameters during ageing

During the lifetime of a lead–acid battery the described ageing mechanisms have an influence on the electrical performance. The parameters changed are influencing the behaviour under open-circuit conditions as well as under load. For any electrical model, the values of the resistances and capacities change over time [46].

Table 16.4 Comparison of the different ageing model approaches and their implications for the parameterization process, the simulation speed, the accuracy of the simulated results and the transferability to new lead–acid battery types/designs and new applications

	Event-oriented	Weighted capacity-throughput	Physicochemical
Parameterization process	Expertize, no tests	Expertize and simplified tests	Literature research and intensive testing
Speed of calculation	High	Medium	Low
Accuracy of the results	Low, no extrapolation	Medium, allows qualitative comparison	High, detailed information
Transfer to new battery type or application	Low, new input necessary	Low, influence factors have to be investigated	High, new battery design as input

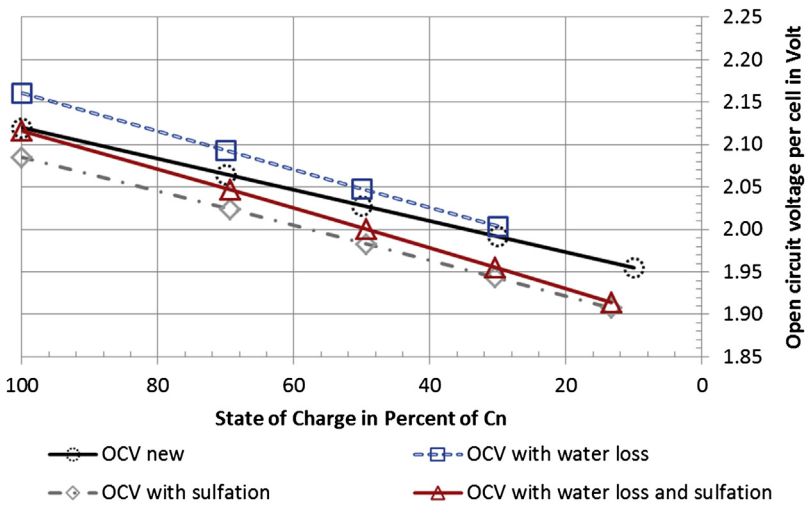

Figure 16.17
Calculated change of open-circuit voltage (OCV) (start: *black solid line*) with assumed water loss (*blue dashed line*) and sulfation (*grey dashed line*). For reasons of simplicity the relation between state-of-charge and OCV has been assumed to be linear. This is not completely accurate but gives a good indication for the process over a lifetime.

The theoretical OCV of a lead–acid cell changes due to the effect of water loss and sulfation, which is illustrated in Fig. 16.17. The black solid line represents the OCV curve at the beginning of lifetime. For reasons of simplicity the relation between SoC and OCV has been assumed to be linear. This is not

totally accurate but gives a good indication for the process over lifetime. A loss of water changes the acid density resulting in an increased cell voltage with a steeper slope over the SoC (blue dashed line) while sulfation changes the amount of H_2SO_4 in the solution and thus decreases the cell voltage (grey dashed line). The red line depicts an overlay of the two effects here with a 20%-loss of H_2SO_4 to sulfation.

The decreasing available capacity over life is due to increased overpotentials under equal loads. This is, on the one hand, due to an increased ohmic resistance because of a higher share of lead sulfate in the AM as well as possible passivating layers of the corrosion. Additionally, a decreased overall acid concentration due to sulfation leads to an on average lower voltage level. On the other hand, the loss of active-material or decreased active surface through shedding or sulfation, respectively, leads to a higher charge-transfer resistance.

Abbreviations, acronyms and initialisms

AGM Absorptive Glass-Mat (valve-regulated lead–acid battery)
AM Active-mass (NAM, Negative active-mass, PAM, Positive active-mass)
BSD Battery State Detection
CFD Computational fluid dynamics
COS Cast-on-straps
DoD Depth-of-discharge
EEC Equivalent Electrical Circuit
EFB Enhanced Flooded Battery (also referred to as IFB = improved flooded battery)
EIS Electrochemical Impedance Spectroscopy
EoL End-of-life
HiL Hardware-in-the-loop
OCV Open-Circuit Voltage
PDE Partial differential equations
PSoC Partial state-of-charge
SLI Starting-lighting-ignition
SoC State-of-charge
SoF State-of-function
SoH State-of-health
VRLA Valve-regulated lead–acid battery

References

[1] W. Peukert, Elektrotech. Zeitschrift 18 (1897) 287–288.
[2] J.E.B. Randles, Discuss. Faraday Soc. 1 (1947) 11.
[3] C.M. Shepherd, J. Electrochem. Soc. 112 (1965) 657.
[4] J. Schiffer, D.U. Sauer, H. Bindner, T. Cronin, P. Lundsager, R. Kaiser, J. Power Sources 168 (2007) 66–78.
[5] K.J. Euler, Electrochim. Acta 13 (1968) 1533–1549.

[6] W. Tiedemann, J. Newman, J. Electrochem. Soc. 122 (1975) 1482–1485.
[7] W.G. Sunu, in: White (Hg.) – Electrochemical Cell Design, 1984, pp. 357–376.
[8] H. Gu, T.V. Nguyen, R.E. White, J. Electrochem. Soc. 134 (1987) 2953–2960.
[9] P. Ekdunge, D. Simonsson, J. Appl. Electrochem 19 (1989) 136–141.
[10] D. Simonsson, J. Electrochem. Soc. 120 (1973) 151–157.
[11] W.B.C. Gu, Y. Wang, B.Y. Liaw, J. Electrochem. Soc. 144 (1997) 2053.
[12] D.U. Sauer, J. Power Sources 64 (1997) 181–187.
[13] J.J. Lander, J. Electrochem. Soc. 103 (1956) 1–8.
[14] H. Metzendorf, J. Power Sources 7 (1982) 281–291.
[15] W. Kappus, Electrochim. Acta 28 (1983) 1529–1537.
[16] A. Winsel, E. Voss, U. Hullmeine, in: Proceedings of the International Conference on Lead/Acid Batteries:LABAT '89, 30, 1990, pp. 209–226.
[17] A. Winsel, E. Bashtavelova, J. Power Sources 46 (1993) 211–217.
[18] E. Meissner, J. Power Sources 78 (1999) 99–114.
[19] M. Kramer, J. Electrochem. Soc. 131 (1984) 1283.
[20] D.M. Bernardi, J. Electrochem. Soc. 137 (1990) 1670.
[21] D.M. Bernardi, J. Electrochem. Soc. 140 (1993) 2250.
[22] D.M. Bernardi, M.K. Carpenter, J. Electrochem. Soc. 142 (1995) 2631–2642.
[23] D.U. Sauer, Optimierung des Einsatzes von Blei-Säure-Akkumulatoren in Photovoltaik-Hybrid-Systemen unter spezieller Berücksichtigung der Batteriealterung, Doktorarbeit, Ulm, 2003.
[24] P. Caselitz, Physikalisches Modell für Starterbatterien zur Bordnetzsimulation von Kraftfahrzeugen, 1996, pp. 219–229.
[25] D.U. Sauer, H. Wenzl, Selected Papers Presented at the 11th ULM ElectroChemical Days 176, 2008, pp. 534–546.
[26] T. Baumhöfer, W. Waag, D.U. Sauer, Specialized battery emulator for automotive electrical systems 2010 IEEE Vehicle Power and Propulsion Conference, Lille, 2010, pp. 1–4.
[27] M. Thele, E. Karden, E. Surewaard, D.U. Sauer, in: Special Issue 6th International Conference LABAT 2005, Varna, Bulgaria and 11th Asian Battery Conference (11 ABC, Ho Chi Minh City, Vietnam), 158, 2006, pp. 953–963.
[28] P. Caselitz, R. Juchem, in: Kasseler Symposium Energie-Systemtechnik '98, Institut für Solare Energieversorgungstechnik, 1998, pp. 142–149.
[29] F. Mattera, D. Desmettre, J.L. Martin, P. Malbranche, in: Proceedings of the International Conference on Lead–Acid Batteries, LABAT '02, 113, 2003, pp. 400–407.
[30] M. Huck, J. Badeda, D.U. Sauer, J. Power Sources 279 (2015) 351–357.
[31] D. Berndt, U. Teutsch, J. Electrochem. Soc (1996) 790–798.
[32] J. Newman, J. Electrochem. Soc. 144 (1997) 3081.
[33] W.B. Gu, G.Q. Wang, C.Y. Wang, in: Sixteenth Annual Battery Conference on Applications and Advances, 2001, pp. 181–186.
[34] M. Thele, A Contribution to the Modelling of the Charge Acceptance of Lead–Acid Batteries – Using Frequency and Time Domain Based Concepts, Dissertation, Aachen, 2008.
[35] E. Barsoukov, J.R. Macdonald, Impedance Spectroscopy: Theory, Experiment, and Applications, second ed., Wiley-Interscience, A John Wiley & Sons, Inc. publication, Hoboken, New Jersey, 2005.
[36] F. Alavyoon, A. Eklund, F.H. Bark, R.I. Karlsson, D. Simonsson, Electrochim. Acta 36 (1991) 2153–2164.
[37] J. Kowal, D. Schulte, D.U. Sauer, E. Karden, J. Power Sources 191 (2009) 42–50.
[38] S. Schaeck, A.O. Stoermer, E. Hockgeiger, J. Power Sources 190 (2009) 173–183.
[39] E. Karden, S. Ploumen, B. Fricke, T. Miller, K. Snyder, J. Power Sources 168 (2007) 2–11.

[40] S. Schaeck, A.O. Stoermer, F. Kaiser, L. Koehler, J. Albers, H. Kabza, J. Power Sources 196 (2011) 1541–1554.
[41] D. Pavlov, in: J. Garche (Ed.), Encyclopedia of Electrochemical Power Sources, Academic Press, 2009, pp. 610–619.
[42] P. Ruetschi, J. Power Sources 127 (2004) 33–44.
[43] D. Berndt, J. Power Sources 100 (2001) 29–46.
[44] D.U. Sauer, in: J. Garche (Ed.), Encyclopedia of Electrochemical Power Sources, Academic Press, 2009, pp. 805–815.
[45] E. Meissner, G. Richter, J. Power Sources 144 (2005) 438–460.
[46] G. Pilatowicz, H. Budde-Meiwes, D. Schulte, J. Kowal, Y. Zhang, X. Du, M. Salman, D. Gonzales, J. Alden, D.U. Sauer, J. Electrochem. Soc. 159 (2012) A1410–A1419.
[47] J. Badeda, J. Kabzinski, D. Schulte, H. Budde-Meiwes, J. Kowal, D.U. Sauer, in: Advanced Battery Power – Kraftwerk Batterie, Aachen, Germany, 2013.
[48] M. Cugnet, S. Laruelle, S. Grugeon, B. Sahut, J. Sabatier, J.-M. Tarascon, A. Oustaloup, J. Electrochem. Soc. 156 (2009) A974.
[49] S.S. Misra, A.J. Williamson, Proc. Int. Telecommunications Energy Conference (INTELEC), 1995, pp. 360–363.